

Theory and practice of proximity correction by secondary exposure

Todd K. Leen^{a)}

IBM, General Technology Division, Essex Junction, Vermont 05452

(Received 14 March 1988; accepted for publication 25 October 1988)

This article examines the theory and practice of correcting proximity effect in direct write electron beam lithography by the introduction of a second diffuse, image-complement exposure. The common point-spread function for energy deposition in the substrate is used in formulating a solution to the inverse scattering problem, and the solution is expressed as a power series in the backscatter coefficient. The ghost technique is shown to constitute an approximation to this solution. This mathematical exposition clearly indicates the power of the technique for providing very accurate, point-by-point correction of proximity effect. Application of the procedure to nonlinear resists in a shaped-beam exposure tool is given.

I. INTRODUCTION

Electron beam lithography suffers from degradation of image size uniformity by scattering of the incident beam from the substrate back into the resist. The developed image sizes thus depend on the pattern written in the vicinity of a given shape, as well as the spatial region intentionally written. This proximity effect can be quite pronounced in submicron lithography on silicon¹⁻⁵ or in coarser structures printed over high z substrates (e.g., optical lithography masks). The techniques used to correct for proximity effect include the following: adjustment of linewidths,³⁻⁵ local adjustment of the dose applied to subsets of shapes,⁵⁻⁷ and the ghost technique discussed here.^{8,9} Of the three, only the last is free of the need for extensive computational overhead.

In Sec. II we review the relevant imaging theory and develop a solution to the inverse scattering problem, i.e., what pattern needs to be written in order to obtain a desired energy distribution within the resist. This solution breaks naturally into a power series in the backscatter energy coefficient, η . The ghost technique is shown to be an approximation to the exact solution. The mathematical exposition thus provides for comparison between the present technique, and a (fictitious) perfectly implemented proximity correction. We explicate this comparison in the configuration space (energy deposition as a function of position within the pattern) and show how the quality of correction varies with perturbations of the experimental parameters. We believe that the configuration space analysis provides a more intuitive ground for assessing the accuracy of the correction than does the Fourier space treatment (discussing the modulation transfer function) of Ref. 9.

Finally, in Sec. III, results are given for the technique as practiced on a shaped-beam exposure tool. The principle results of this note are the new theoretical description of ghost proximity correction and its application to nonlinear resist systems.

II. e-BEAM IMAGING THEORY AND GHOST PROXIMITY CORRECTION

When an isolated shape is written with a uniform dose, all regions of the shape receive, through backscatter, energy initially directed at other portions of the shape. This backscatter effect falls off with distance from the beam center. Consequently, the central region of a shape receives more backscattered radiation than the peripheral areas. This variation of energy deposition through the shape is commonly known as intrashape proximity effect. In the ghost technique, the areas outside the shape are written at a reduced dose with a defocused beam. The tail of this diffuse secondary image penetrates the periphery of the shape and thus elevates the energy deposited at the edge. If the dose and beam spread of the secondary exposure are correctly chosen, one obtains a nearly flat energy deposition both internal and external to the shape. Although this discussion addresses only intrashape effects, it will be clear from the development below that the technique corrects all exposure variations due to backscatter independent of the particular geometry of the shapes written. Figures 1(a) and 1(b) illustrate how the above discussed fill occurs.

For simplicity, we ignore the depth dependence of the energy deposition in the resist and concentrate only on the remaining two spatial degrees of freedom. This approximation corresponds to an averaging of the vertical energy profile, or alternately to concentrating attention on a single depth at which the imaging is arbitrarily defined. One assumes that the energy deposition is a linear function of the pattern written and thus defines a point-spread function which is the energy distribution in the resist corresponding to a delta function pattern. We assume the point-spread function to be given by the now familiar sum of two Gaussians,

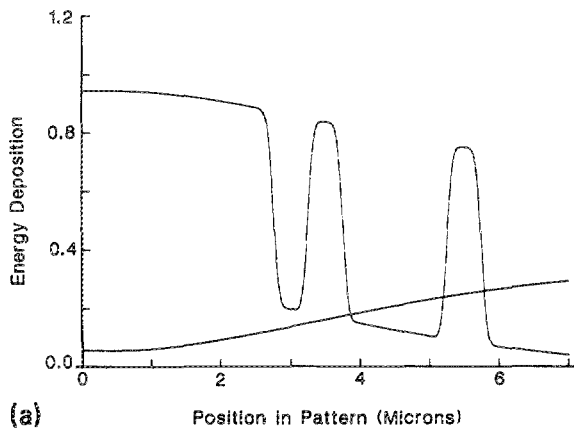
$$h(x) = (1/1 + \eta) [g_\alpha(x) + \eta g_\beta(x)], \quad (1a)$$

where

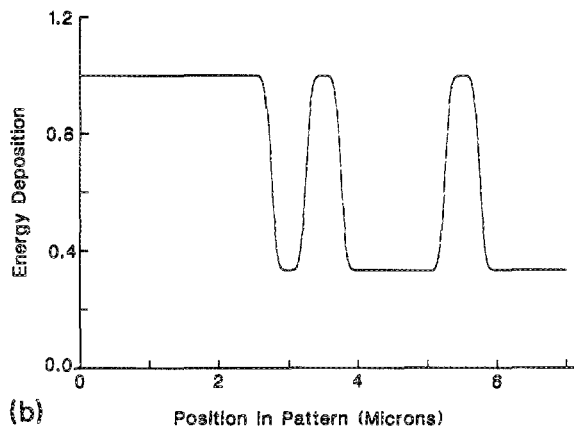
$$g_\alpha(x) = (1/\pi\alpha^2) \exp - (x/\alpha)^2, \quad (1b)$$

and $\beta \gg \alpha$.^{1,2} We assume that the beam edge slope (or Gaus-

^{a)} Present address: Robert Dow Neurological Sciences Institute, 1120 N.W. 20th Avenue, Portland, OR 97209.



(a) Position in Pattern (Microns)



(b) Position in Pattern (Microns)

FIG. 1. (a) Energy deposition in resist resulting from primary and secondary exposures. The primary exposure carries the pattern details while the secondary exposure provides the fill to correct for proximity effect. (b) Summation of the two curves of (a) showing uniform energy distribution for all pattern areas.

sian width of the beam) has been convoluted into these functions so that the first term in Eq. (1a) represents the effects of both forward scatter and beam dispersion. The second term similarly reflects both backscatter and beam dispersion, although the latter is negligibly small in relation to the former. The first term in Eq. (1a) generates the resolution limit or high-frequency cutoff of the system. The second term generates proximity effect. The modulation transfer function (MTF) dual to the point spread of Eq. (1) is

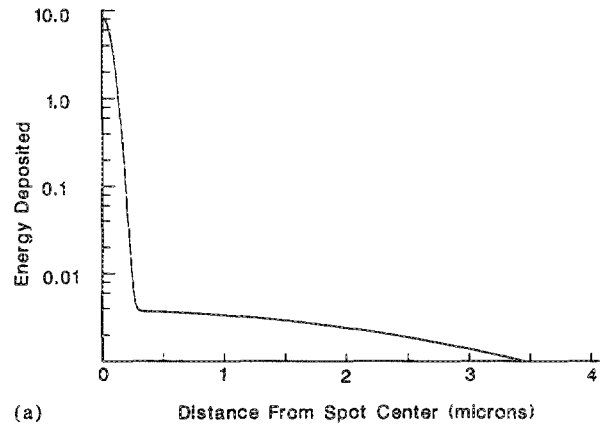
$$H(\lambda) = \left(\frac{1}{1 + \eta} \right) \left[\exp - \left(\frac{\pi\alpha}{\lambda} \right)^2 + \eta \exp - \left(\frac{\pi\beta}{\lambda} \right)^2 \right], \quad (1c)$$

where λ is the spatial wavelength. The point spread and corresponding MTF are plotted in Fig. 2. One clearly sees the high-frequency cutoff imposed by alpha as well as the low-frequency rise in the MTF responsible for proximity effects. As pointed out in Ref. 10, correction for proximity effect corresponds to eliminating this low-frequency shift in the MTF.

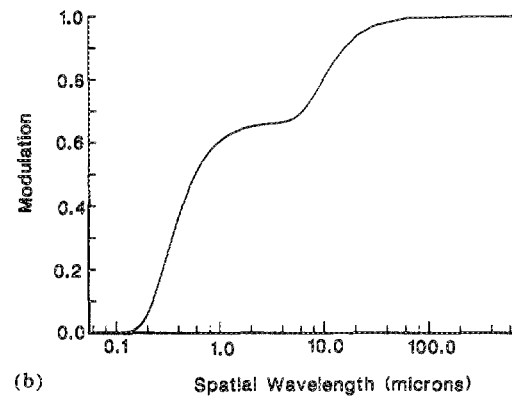
The energy deposited in the resist is proportional to the convolution of the pattern function (intensity versus position) with the point spread of Eq. (1). Accordingly, we define an energy distribution function given by

$$d(x) = p(x) * h(x), \quad (2)$$

where "*" denotes convolution and $p(x)$ is the pattern func-



(a) Distance From Spot Center (microns)



(b) Spatial Wavelength (microns)

FIG. 2. (a) Point-spread function of Eq. (1a). The central peak corresponds to the forward scatter in the resist and the finite beam slope. The tail is the backscattered energy profile. The vertical scale is arbitrary. (b) Modulation transfer function corresponding to the point spread of (a).

tion. For now, the pattern function is considered to take values between zero and one (beam off, beam on). In the ghost correction technique, a second exposure is made using the complement of the primary pattern exposed at a reduced dose R with a defocused beam. We treat the defocused beam as Gaussian,

$$g_b(x) = (1/\pi b^2) \exp - (x/b)^2. \quad (3)$$

The secondary exposure is thus described by the pattern function

$$p_2(x) = R [1 - p(x)] * g_b(x), \quad (4a)$$

and deposits energy in the resist,

$$d_2(x) = R [1 - p(x)] * g_b(x) * h(x). \quad (4b)$$

Carrying out the indicated convolutions, and combining Eqs. (2) and (4b), one easily finds the total deposited dose:

$$d_g(x) = R + (p * g_\alpha) / (1 + \eta) + [p / (1 + \eta)] \times * [\eta g_\beta - R (g_{\sqrt{\alpha^2 + b^2}} + \eta g_{\sqrt{\beta^2 + b^2}})]. \quad (5)$$

The beam spread b and the dose ratio R are adjusted so that the terms in square brackets in Eq. (5) sum approximately to zero. This is most nearly accomplished by setting the integral and the peak of these terms equal to zero, resulting in

$$R = \eta / (1 + \eta), \quad (6a)$$

$$b = \eta / (1 + \eta)^{1/4}, \quad (6b)$$

as in Ref. 9. With the parameters of Eq. (6), the net pattern written in the ghost scheme assumes the form

$$p_g = p + (\eta/1 + \eta)(1 - p) * g_b, \quad (7)$$

where the first term represents the principle exposure, and the second the complementary exposure.

This prescription is, in fact, an approximate solution to the proximity equations in the following sense. Equation (2) may be formally inverted to find the pattern function corresponding to a desired energy distribution $d(x)$,

$$p(x) = d(x) * h^{-1}(x). \quad (8)$$

The quickest route to explicate this inversion is to Fourier transform Eq. (2) and use the convolution theorem. Hence,

$$D(k) = P(k)H(k), \quad (9)$$

and its inversion is simply

$$P(k) = D(k)/H(k), \quad (10)$$

where $k = 2\pi/\lambda$ and P , D , and H are the transforms of p , d , and h , respectively. At low spatial wavelengths (large k), the MTF is dominated by the drop in the alpha (α) term of Eq. (1c). As k increases $H(k)$ approaches zero and the pattern transform $P(k)$ thus diverges. Thus, the use of (10) to generate a pattern function $p(x)$ would result in divergent high-frequency oscillations in the solution. Physically, Eq. (10) tries to restore the high-frequency information lost due to forward scatter and finite beam width. The high-frequency divergence in $P(k)$ may be removed by multiplying it by $G_\alpha(k)$, the transform of the first term of Eq. (1a). This corresponds to convolving the pattern function with $g_\alpha(x)$ and thus recovering the forward scatter/beam spread contribution of the point-spread function. The regularized pattern function thus becomes

$$P'(k) = D(k)/(1 + \eta) [1 + \eta G_\beta(k)/G_\alpha(k)], \quad (11)$$

with

$$G_\beta/G_\alpha = \exp - (k/2)(\beta^2 - \alpha^2). \quad (12)$$

In the limit $k \rightarrow \infty$, the ratio G_β/G_α approaches zero so that the rescaled pattern function $P'(k)$, given by Eq. (11), remains bounded. The regularized pattern function of Eq. (11) may be expanded in a power series in eta, and one recovers the form

$$P'(k) = (1 + \eta)D(k) \sum_{N=0}^{\infty} (-\eta)^N G_{\sqrt{N(\beta^2 - \alpha^2)}}(k). \quad (13)$$

Finally, Eq. (13) may be transformed back into the configuration space using the convolution theorem to give

$$p'(x) = (1 + \eta)d(x) * \sum_{N=0}^{\infty} (-\eta)^N g_{\sqrt{N(\beta^2 - \alpha^2)}}(x). \quad (14)$$

[For an alternate derivation of Eq. (14), see (10).] It is straightforward to see that convolution of $p'(x)$ with the point-spread function of Eq. (1a) yields a dose deposited in the resist given by

$$d'(x) = d(x) * g_\alpha(x). \quad (15)$$

Hence, one may regard Eq. (14) as a solution to the proximity equation to within the resolution limits imposed by forward scatter and beam slope.

The relations amongst the functions $d(x)$, $d'(x)$, and $p'(x)$ are depicted in Fig. 3. In the regions in which d is zero, corresponding to no energy deposition, the pattern $p'(x)$ is required to make negative excursions. This is, of course, unphysical, but is required to cancel the energy scattered into these regions from nearby shapes. One can relax this requirement on the pattern function by requiring the energy deposition $d(x)$ to drop to a nonzero, but acceptably small, value between the shapes to be printed. To make contact with the ghost approach, we rescale the desired energy deposition according to

$$d \rightarrow (\eta + d)/(\eta + 1). \quad (16)$$

This rescaling leaves an energy deposition which ranges from $(\eta/1 + \eta)$ to unity. The pattern function corresponding to this rescaled energy deposition follows from Eq. (14). Combining (14) and (16) and using the fact that $\beta \gg \alpha$, one recovers

$$p'(x) = (\eta/1 + \eta) + d - \eta d * g_\beta + \eta^2 d * g_{\beta/\sqrt{2}} + \dots \quad (17)$$

The relation of this full solution to the ghost prescription is revealed by rewriting the pattern function for the latter from Eq. (7) in the form

$$p_g(x) = (\eta/1 + \eta) + d - \eta d * g_b + \eta^2 d * g_b + \dots, \quad (18)$$

having expanded the coefficient of the convolution term of Eq. (7) as a power series in η , and replacing p with d .

The leading two terms of (17) and (18) represent the constant background and the uncorrected pattern, respectively. The third term represents the lowest order (in eta) proximity correction.

As an illustration of the degree to which the ghost-scheme approximates the exact solution, an example of the pattern functions for Eqs. (17) and (18) are plotted in Fig. 4(a). The curve for the exact solution has been calculated to the eighth order in η while that for the ghost pattern is shown to all orders. The normalized difference between the two solutions, $(p' - p_g)/p'$, for the same pattern is shown in Fig. 4(b). The energy doses deposited in the resist (i.e., the convolution of p' and p with the point-spread function) for these cases is shown in Fig. 5(a), and the normed difference

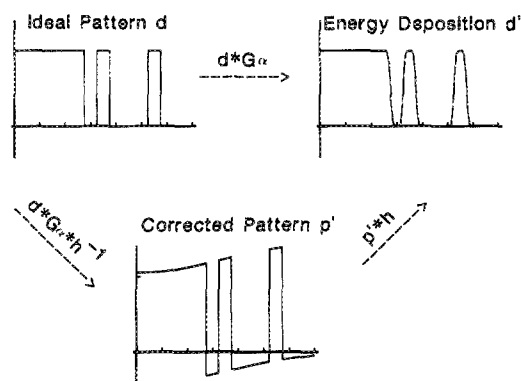
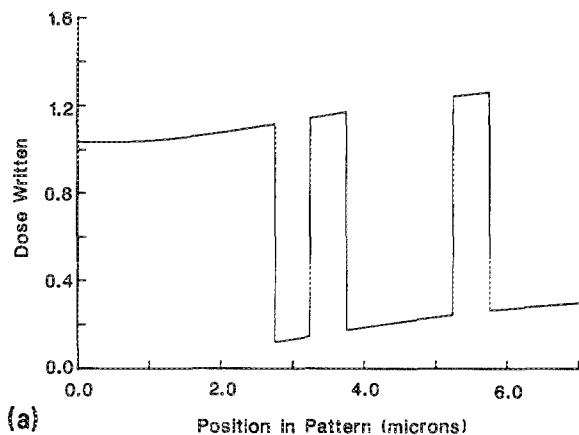
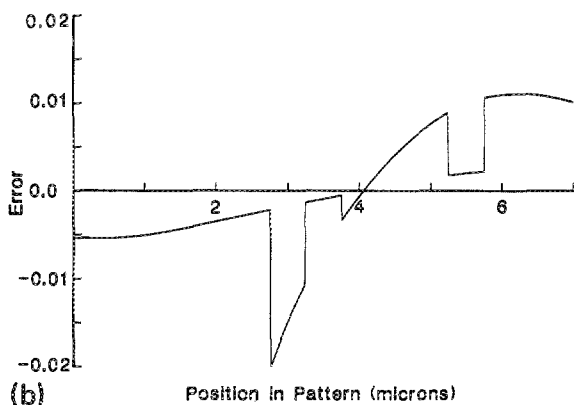


FIG. 3. Relations between the ideal energy deposition d , the corrected pattern function $p'(x)$, and the actual energy deposition $d'(x)$ resulting from the corrected pattern.



(a) Fully corrected and ghost corrected pattern functions (p' and p_g) from Eqs. (17) and (18), respectively.

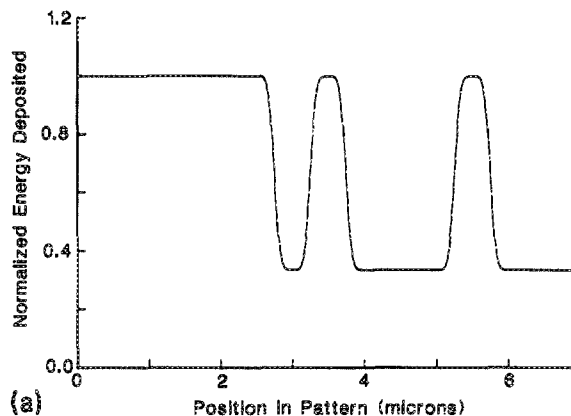


(b) Relative error between p' and p . Plotted function is $(p' - p_g)/p'$.

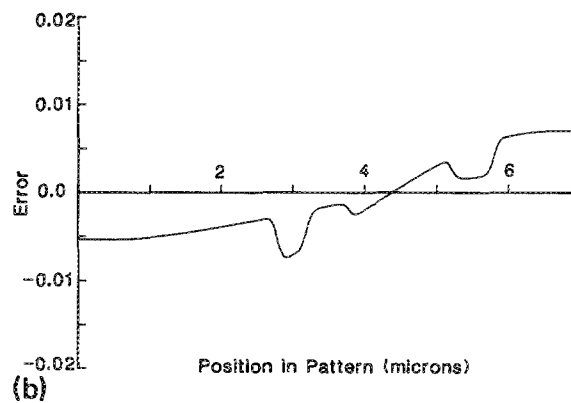
FIG. 4. (a) Fully corrected and ghost corrected pattern functions (p' and p_g) from Eqs. (17) and (18), respectively. (b) Relative error between p' and p . Plotted function is $(p' - p_g)/p'$.

$(d' - d_g)/d'$ is plotted in Fig. 5(b). As a comparison, the energy deposited by the uncorrected pattern is shown in Fig. 5(c). We note the accuracy of the ghost prescription, particularly for the deposited energy distributions of Fig. 5(b).

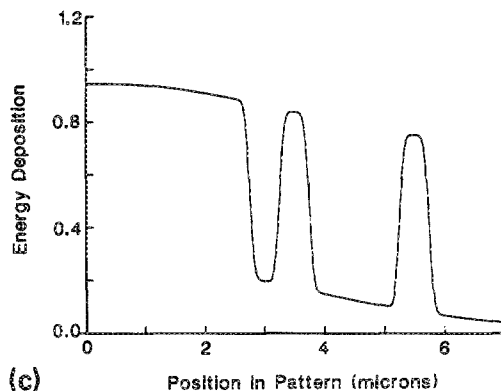
Since the ghost technique is a point-by-point procedure, it offers more accurate correction than techniques based upon averaging doses over finite regions. One needs, however, to pick the parameters R and b of Eq. (6) with some care. As a brief illustration of the effects of errors in the parameter assignment, we give the energy distribution functions for several examples of R and b departing from those given in Eqs. (6). Figure 6(a) shows the energy deposition resulting from the three values of dose ratios as follows: $R = 0.8R_0$, $R = R_0$, and $R = 1.2R_0$, with R_0 the value dictated by Eq. (6a). Since R is monotonic increasing in η , these three values represent, respectively, underestimate, correct estimate, and overestimate of η . Stated differently, the three choices represent undercorrection, correction, and overcorrection for the proximity effect. As expected, undercorrection results in the narrow isolated feature receiving less energy than the others—qualitatively similar to the uncorrected case in Fig. 5(c). Conversely, the overcorrected version deposits too much energy in the isolated feature. Experimentally, one would observe narrowing (widening) of the isolated feature relative to the rest of the pattern for the undercorrected (overcorrected) choices of the dose ratio. Similarly, Fig. 6(b) illustrates the effects of choosing the



(a) Fully corrected and ghost-corrected energy deposition functions (d' and d_g) corresponding to the patterns of Fig. 3(a).



(b) Relative error in energy deposition. Plotted function is $(d' - d_g)/d'$.



(c) Uncorrected energy deposition.

FIG. 5. (a) Fully corrected and ghost-corrected energy deposition functions (d' and d_g) corresponding to the patterns of Fig. 3(a). (b) Relative error in energy deposition. Plotted function is $(d' - d_g)/d'$. (c) Uncorrected energy deposition.

beam width b for the secondary exposure; the three values are as follows: $b = 0.8b_0$, $b = b_0$, and $b = 1.2b_0$, with b_0 the value prescribed by Eq. (6b). One sees that choice of beam width is less critical than picking the correct dose ratio. This is particularly fortunate for implementation in a shaped-beam tool, as the beam dispersion varies somewhat with the choice of spot size. In practice, one estimates β and η from Monte Carlo simulations of electron scattering and energy absorption in the resist/substrate in use, and uses these to estimate R and b via Eqs. (6). Initial exposures with these parameters will then indicate necessary adjustments for subsequent exposures.

In addition to imperfect choice of dose ratio and beam spread, the relative alignment between the primary and secondary exposures also affects the quality of the proximity

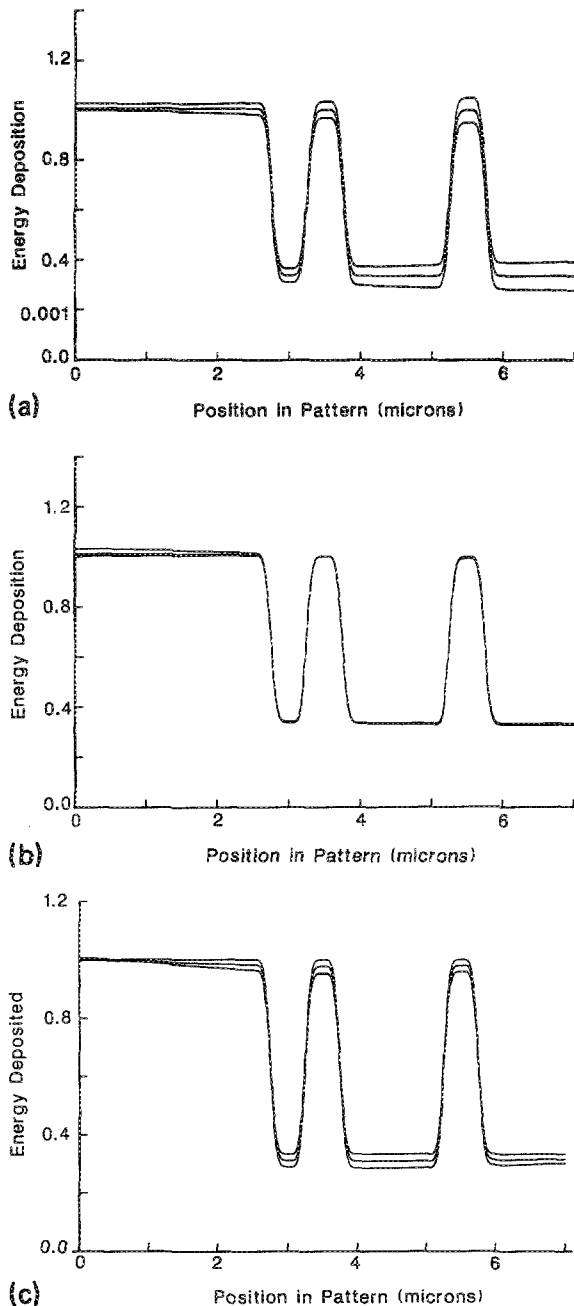


FIG. 6. Energy deposition resulting from ghost-corrected exposures using values of dose ratio R or beam spread b differing from those prescribed by Eqs. (6). (a) Use of incorrect dose ratio R . The curves represent, from top to bottom: $R = 1.2R_0$, $R = R_0$, and $R = 0.8R_0$, where R_0 is the value specified by Eq. (6a). (b) Use of incorrect beam spread b . The curves represent, from top to bottom: $b = 0.8b_0$, $b = b_0$, and $b = 1.2b_0$, where b_0 is the value specified by Eq. (6b). (c) Effect of misalignment between primary and secondary exposures. The three energy deposition profiles plotted correspond to (top to bottom): 0.0, 0.5, and 1.0 μm offset, respectively.

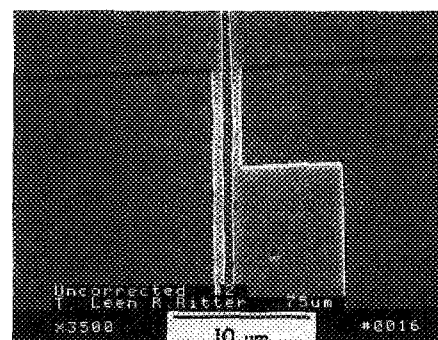
correction. Fortunately, since the second exposure is carried out with a diffuse beam, placement of the second image relative to the first is not critical. This holds important consequences for possible extensions of the technique to be alluded to in the summary section below. Figure 6(c) portrays the energy deposition resulting from relative offsets of 0.0, 0.5, and 1.0 μm between the primary and secondary exposures. The error introduced into the correction is of similar magni-

tude to that observed in Fig. 5(a). As the minimum dimensions in the examples shown are 0.5 μm , an offset of the order of 1.0 μm is quite large, and certainly well outside the precision accessible to electron beam lithography. Thus, one sees that the technique is very robust against alignment errors between the two images. The placement of the secondary image is not critical precisely because it is projected with a diffuse beam.

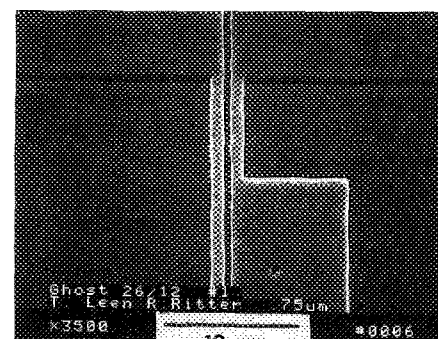
III. RESULTS

We have implemented the ghost scheme on the IBM EL-3 shaped-beam exposure tool as modified for 0.5 μm lithography.¹¹ Substrates were prepared with oxide/nitride deposition over silicon, and fiducial marks etched for each chip prior to resist coating. These targets provide for accurate registration between the primary and complementary exposures. Wafers were coated with a 0.5- μm film of diazosensitized novalak resin resist. This use of a highly nonlinear resist system extends previously reported results implementing the scheme on polymethyl methacrylate resist.^{8,9} The resist-coated wafers were baked at 85 $^\circ\text{C}$ for 30 min and stored under refrigeration prior to exposure and development.

The exposure pattern employed includes a variety of line-space arrays as well as geometrically complex structures designed to reveal variations due to proximity effect. The primary pattern was exposed at a dose of 20 $\mu\text{C}/\text{cm}^2$ at a nominal beam edge slope of 0.13 μm .¹⁰ The complementary pattern was exposed at a range of doses with a beam edge slope equivalent to a 3.0 μm Gaussian width. Development time was controlled by endpoint detect on a large site in the



(a)



(b)

FIG. 7. Micrograph of patterns exposed with (a) no correction applied, and (b) ghost proximity correction. Lines and spaces in the example are 0.75 μm features.

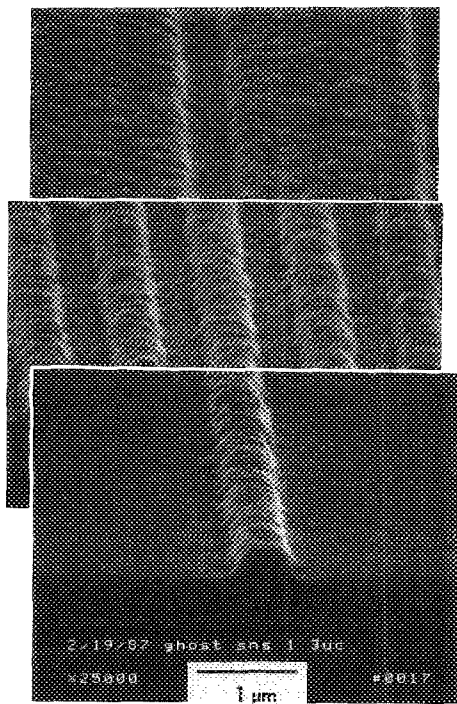


FIG. 8. Composite electron micrograph of (top to bottom) isolated line, line-space array, and isolated space, all of $0.5 \mu\text{m}$ dimension.

center of each wafer. This site received a blanket exposure of $20 \mu\text{C}/\text{cm}^2$ during the primary pattern exposure, and no radiation during the secondary exposure.

Figures 7(a) and 7(b) show, respectively, uncorrected and ghost-corrected exposures on representative structures within the test chip. Principle to this discussion is the long vertical line passing through the center of each photo. This feature passes through three differing environments: (1) the isolated portion at the top of each photo, (2) the central portion flanked by two large exposed regions, and (3) the lower portion flanked by one exposed region. The linewidth and bordering spaces, as well as the contact hole visible at the bottom right of the center, were designed to $0.75 \mu\text{m}$ dimensions in each case. In the uncorrected example, the vertical line blossoms significantly in the region where it is flanked by the two larger shapes, illustrating the intershape proximity effect. This line also narrows noticeably in the isolated region at the top of the photo. In addition, the corners of the larger shapes nearest to the central line bow outward, increasing the gap size in the region. This is the result of a lack of backscattered energy in these areas relative to the remainder of the large shapes, and well illustrates intrashape proximity effect. In the corrected example of Fig. 7(b), these problems are well controlled, with both linewidth uniformity and corner squareness much improved.

Extending the practice to higher-resist sensitivity, we have implemented the scheme on an IBM proprietary sulfone resist operating at a primary exposure dose of $3.5 \mu\text{C}/\text{cm}^2$. A result from those experiments is shown in the photomicrographs of Fig. 8. This composite photograph shows $0.5\text{-}\mu\text{m}$ features including isolated line, line-space array and an isolated space. The composite shows good control of the feature size throughout the varying environments.

IV. SUMMARY

The ghost technique for correction of proximity effect in electron beam lithography has been shown to be an approximate realization of the exact solution to the pertinent imaging equations. The effects of errors in the dose and beam spread employed during the complementary exposure have been explored for a representative energy deposition function. Energy deposition is found to be more sensitive to variations in dose ratio than to variations in beam spread. Alignment between the primary and secondary images is found to be noncritical.

The technique has been applied to nonlinear resist systems exposed in a shaped-beam tool with good results, extending previous work on linear resist systems.

The principal drawback of the technique is the requirement for two exposures of each wafer. The fact that the secondary exposure is carried out at a reduced dose does alleviate the problem somewhat. It is difficult to estimate the total exposure time in general since this is highly dependent on the percentage of the die area that is written by the primary pattern, and the manner in which the shapes are partitioned. For the test chips used in this study, the total write time for both images on the sulfone resist measured 25 min, 15 s. In comparison, the time necessary to write the same patterns with dose-compensation proximity correction measured 12 min, 0 s.

It seems likely that some modification of the technique to reduce write time and retain good proximity correction is possible. Since the secondary exposure is carried out with a diffuse beam, and its alignment to the primary pattern is not critical, the full resolution and overlay capabilities of electron beam lithography are not required. We envision performing the secondary exposure with, say, an optical tool to increase efficiency. Alternately, one might write the secondary pattern somewhat coarsely, departing from strict complementarity to the primary pattern, and realize a savings in time.

Note added in proof: The principle exposure p of Eq. (7) is the *desired* energy deposition d . Hence the substitution in Eq. (18).

ACKNOWLEDGMENTS

The author takes pleasure in acknowledging the contribution of Cecilia Tsai in carrying out some of the experimental work in the author's absence. Leon Moszkowicz and Rick Ritter aided in analysis of the samples. I thank Nick Eib and Mike Rosenfeld for stimulating conversation and critique. Finally, Sherry Gillespie provided the environment under which this work was carried out and an initial reading of the manuscript.

¹D. F. Kyser and C. H. Ting, *J. Vac. Sci. Technol.* **16**, 1759 (1979).

²M. Parikh, *IBM J. Res. Dev.* **24**, 438 (1980).

³H. Sewell, *J. Bacteriol. Sci. Technol.* **15**, 927 (1978).

⁴M. Parikh, *J. Appl. Phys.* **51**, 705 (1980).

⁵M. Parikh, *J. Appl. Phys.* **50**, 4371 (1979).

⁶J. S. Greeneich, *J. Vac. Sci. Technol.* **19**, 1269 (1981).

⁷F. Murai, S. Okazaki, Y. Takeda, and H. Obayashi, *IEDM Tech. Dig.*, 558 (1983).

⁸G. Owen and P. Rissman, *J. Appl. Phys.* **54**, 3573 (1983).

⁹G. Owen, P. Rissman, and M. Long, *J. Vac. Sci. Technol.* **B3**, 153 (1985).

¹⁰P. D. Gerber, *J. Vac. Sci. Technol.* **B6**, 432 (1988).

¹¹D. E. Davis, S. J. Gillespie, and W. Stickel, *J. Vac. Sci. Technol.* **B1**, 1003 (1983).